2024 European Control Conference (ECC)
June 25-28, 2024. Stockholm, Sweden

Unknown Input Observer for Temperature Profile Estimation in Systems with Unknown Heat Fluxes

Helmut Niederwieser[1], Stefan Koch[2] and Markus Reichhartinger[3]

Abstract— **This article demonstrates the application of a recently proposed sliding mode observer concept for linear time-invariant multivariable systems with unknown inputs. In contrast to other sliding mode approaches, this observer concept does neither unnecessarily increase the observer order beyond the plant order nor requires bounded state variables or some restrictive relative degree conditions. This work aims for estimating the temperature profile along an aluminium rod, which is excited with heat fluxes unknown to the observer. The plant model is transformed into a suitable form for observer design, facilitating a straightforward sliding mode observer design. Experimentally obtained estimation results confirm the effectiveness of the observer in a practical application.**

I. Introduction

Estimating unknown system states from measured quantities is key for solving numerous practical control engineering problems. Outside the domain of control systems design, state estimation challenges emerge in various scenarios, including real-time process monitoring, fault detection and isolation, and soft sensing. Typically, designing a state observer requires an accurate model of the plant. However, model uncertainties and external disturbances, regarded as unknown system inputs, introduce additional challenges.

Sliding mode based observers have attracted considerable attention due to their ability of estimating the states theoretically exact in the presence of unknown inputs, provided that certain conditions regarding the system and unknown inputs are met. In recent years, several sliding mode based observer concepts have been introduced based on the principle of the so-called robust exact differentiator (RED) [1]. For example, step-by-step sliding mode observers, see e.g [2], as well as the direct application of the RED as a state observer, see [3], are capable of estimating the plant's state theoretically exact provided that the states remain bounded. Observers that do not require the boundedness of the states include the cascaded observers proposed in [4], [5], [6]. These observers consist of a combination of the RED with a classical Luenberger observer. The cascaded structure ensures global convergence of the estimation error to zero also in the case of unbounded state variables. However, the cascaded observers have at least twice the order of the plant model and also a large number of interdependent tuning parameters. If the so-called observer matching condition [7, Theorem 1.6] is met, earlier approaches such as conventional first-order sliding mode based methods [8], [9] as well as classical Luenberger like observers [7], [10] provide exact estimates of the states in the presence of unknown inputs. The observers based on Luenberger's classical observability canonical form [11], [12] do not suffer from these drawbacks. However, they require a restrictive relative degree condition w.r.t. the unknown input to be satisfied, see, e.g., [12, Assumption 1].

While the aforementioned approaches, in principle, allow solving various problems, the conditions are frequently overly restrictive or result in a substantial implementation and tuning effort. To overcome these issues a novel observer normal form for strongly observable linear time-invariant (LTI) multivariable systems was proposed in [13]. It allows for the straightforward construction of a higher-order sliding mode observer, that ensures global convergence of the estimation error within finite time in the presence of unknown bounded inputs. However, the practical suitability of this observer has not yet been shown.

The practical application of the approach proposed in [13] is demonstrated in the present work. In particular the temperature profile estimation in a thermal system subject to unknown heat fluxes is considered. The plant dynamics are modelled by means of the diffusion equation which is a parabolic partial differential equation (PDE). Discretizing the PDE and applying model order reduction provide an LTI model suitable for observer design.

The paper is structured as follows: In Section II, the observer normal form [13] is outlined. The considered application is described and the state estimation problem is formulated in Section III. In Section IV the plant model is derived followed by the observer design in Section V. Experimental results are provided in Section VI and Section VII concludes the paper.

Nomenclature

Bold lowercase letters refer to vectors and bold uppercase letters refer to matrices. The vector $\boldsymbol{e}_{i,n}$ is the i^{th} canonical unit vector of dimension n. The elements of the matrices $\mathbf{0}_{j\times k}$ and $\mathbf{1}_{j\times k}$ of dimension $j \times k$ are zeros and ones,

The financial support by the Austrian Federal Ministry of Labour and Economy, the National Foundation for Research, Technology and Development and the Christian Doppler Research Association is gratefully acknowledged.

[1]Helmut Niederwieser is with the Institute of Automation and Control, *Graz University of Technology* and BEST–Bioenergy and Sustainable Technologies GmbH, Graz, Austria helmut.niederwieser@tugraz.at

[2]Stefan Koch is with the Christian Doppler Laboratory for Model-Based Control of Complex Test Bed Systems, Institute of Automation and Control, Graz University of Technology, Graz, Austria

[3]Markus Reichhartinger is with the Institute of Automation and Control, Graz University of Technology, Graz, Austria

respectively. Furthermore, $\boldsymbol{I}_i$ is the $i \times i$ identity matrix and

$$\boldsymbol{J}_i = \begin{bmatrix} \boldsymbol{0} & \boldsymbol{I}_{i-1} \\ 0 & \boldsymbol{0}^{\mathrm{T}} \end{bmatrix}.$$

If the dimensions of the previously introduced matrices and vectors are clear anyway, the respective index might be skipped. For sign preserving power functions the notation $\lfloor \cdot \rceil^{\gamma} = |\cdot|^{\gamma} \mathrm{sign}(\cdot)$ and particularly $\lfloor \cdot \rceil^{0} = \mathrm{sign}(\cdot)$ is used. The time-derivatives $\frac{\mathrm{d}}{\mathrm{d}t}x$ and $\frac{\mathrm{d}^2}{\mathrm{d}t^2}x$ are also denoted by $\dot{x}$ and $\ddot{x}$, respectively. Furthermore, $\mathrm{diag}(\boldsymbol{A}_1, \ldots, \boldsymbol{A}_i)$ refers to a block diagonal matrix with elements $\boldsymbol{A}_1, \ldots, \boldsymbol{A}_i$. The solutions of differential equations with discontinuous right-hand side are understood in the sense of Filippov [14].

II. Unknown Input Observer Design for LTI Multivariable Systems

Consider the LTI system

$$\dot{\boldsymbol{x}} = \boldsymbol{A}\boldsymbol{x} + \boldsymbol{D}\boldsymbol{w}, \quad \boldsymbol{y} = \boldsymbol{C}\boldsymbol{x}, \tag{1}$$

with the state vector $\boldsymbol{x} = \begin{bmatrix} x_1 & x_2 & \ldots & x_n \end{bmatrix}^{\mathrm{T}}$, m unknown inputs $\boldsymbol{w} = \begin{bmatrix} w_1 & w_2 & \ldots & w_m \end{bmatrix}^{\mathrm{T}}$, p measured outputs $\boldsymbol{y} = \begin{bmatrix} y_1 & y_2 & \ldots & y_p \end{bmatrix}^{\mathrm{T}}$ and the constant matrices $\boldsymbol{A} \in \mathbb{R}^{n \times n}$, $\boldsymbol{D} \in \mathbb{R}^{n \times m}$ and $\boldsymbol{C} \in \mathbb{R}^{p \times n}$. Without loss of generality, it is assumed that $\boldsymbol{D}$ and $\boldsymbol{C}$ consist of linear independent columns and rows, respectively. The aim is the estimation of $\boldsymbol{x}$ from the output $\boldsymbol{y}$ in the presence of the possibly time-varying unknown input $\boldsymbol{w}$.

Definition 2.1 (strong observability [7]): System (1) is called strongly observable, if $\boldsymbol{y}(t) = \boldsymbol{0}$ for all $t \geq 0$ implies $\boldsymbol{x}(t) = 0$ for all $t \geq 0$.

If the system is strongly observable, higher-order sliding mode techniques can be applied to estimate the state vector in finite time despite the unknown input $\boldsymbol{w}$.

In the following, a recently proposed sliding mode approach [13] is recalled, which relies on a new normal form for LTI multivariable systems with unknown inputs. Due to this suitable choice of coordinates, all drawbacks mentioned in the introduction are avoided and the subsequent observer design is straightforward.

A. An Observer Normal Form for LTI Multivariable Systems with Unknown Inputs

The observer normal form is briefly recapped in

Definition 2.2 (observer normal form [13]): The system

$$\dot{\bar{\boldsymbol{x}}} = \bar{\boldsymbol{A}}\bar{\boldsymbol{x}} + \bar{\boldsymbol{D}}\boldsymbol{w}, \quad \bar{\boldsymbol{y}} = \bar{\boldsymbol{C}}\bar{\boldsymbol{x}}, \tag{2a}$$

is said to be in observer normal form if the system matrices take the form[1]

$$\begin{aligned} \bar{\boldsymbol{A}} &= \bar{\boldsymbol{A}}^{\star} + \bar{\boldsymbol{\Pi}}\bar{\boldsymbol{C}} + \bar{\boldsymbol{P}}\bar{\boldsymbol{M}}, \\ \bar{\boldsymbol{D}} &= \bar{\boldsymbol{P}} \begin{bmatrix} \bar{\boldsymbol{d}}_1 & \bar{\boldsymbol{d}}_2 & \ldots & \bar{\boldsymbol{d}}_p \end{bmatrix}^{\mathrm{T}}, \\ \bar{\boldsymbol{C}} &= \mathrm{diag}(\boldsymbol{e}_{1,\mu_1}^{\mathrm{T}}, \boldsymbol{e}_{1,\mu_2}^{\mathrm{T}}, \ldots, \boldsymbol{e}_{1,\mu_p}^{\mathrm{T}}), \end{aligned} \tag{2b}$$

[1] See [13] for a less compact but more insightful representation.

where

$$\begin{aligned} &\bar{\boldsymbol{A}}^{\star} = \mathrm{diag}(\boldsymbol{J}_{\mu_1}, \boldsymbol{J}_{\mu_2}, \ldots, \boldsymbol{J}_{\mu_p}), \\ &\bar{\boldsymbol{P}} = \mathrm{diag}(\boldsymbol{e}_{\mu_1,\mu_1}, \boldsymbol{e}_{\mu_2,\mu_2}, \ldots, \boldsymbol{e}_{\mu_p,\mu_p}), \\ &\bar{\boldsymbol{M}} = \left[\begin{array}{cc|cc|c|cc} 0 & \boldsymbol{0}^{\mathrm{T}} & 0 & \boldsymbol{0}^{\mathrm{T}} & \cdots & 0 & \boldsymbol{0}^{\mathrm{T}} \\ 0 & \boldsymbol{\beta}_{1,2}^{\mathrm{T}} & 0 & \boldsymbol{0}^{\mathrm{T}} & \cdots & 0 & \boldsymbol{0}^{\mathrm{T}} \\ 0 & \boldsymbol{\beta}_{1,3}^{\mathrm{T}} & 0 & \boldsymbol{\beta}_{2,3}^{\mathrm{T}} & & 0 & \boldsymbol{0}^{\mathrm{T}} \\ \vdots & \vdots & & & \ddots & \vdots & \\ 0 & \boldsymbol{\beta}_{1,p}^{\mathrm{T}} & \cdots & & 0 & \boldsymbol{\beta}_{p-1,p}^{\mathrm{T}} & 0 \quad \boldsymbol{0}^{\mathrm{T}} \end{array}\right] = \begin{bmatrix} \boldsymbol{0}^{\mathrm{T}} \\ \boldsymbol{\beta}_2^{\mathrm{T}} \\ \boldsymbol{\beta}_3^{\mathrm{T}} \\ \vdots \\ \boldsymbol{\beta}_p^{\mathrm{T}} \end{bmatrix}, \\ &\bar{\boldsymbol{\Pi}} \in \mathbb{R}^{n \times p}, \quad \bar{\boldsymbol{d}}_j \in \mathbb{R}^{m}, \quad \boldsymbol{\beta}_{i,j} \in \mathbb{R}^{\mu_i - 1}, \end{aligned} \tag{2c}$$

are constant and $\mu_1, \mu_2, \ldots, \mu_p \in \mathbb{N}$ satisfy $\sum_{j=1}^{p} \mu_j = n$.

In observer normal form, the system is composed of p coupled chains of integrators of orders $\mu_1, \mu_2, \ldots, \mu_p$, each with a single output. The dynamic matrix $\bar{\boldsymbol{A}}$ consists of three parts:

- The matrix $\bar{\boldsymbol{A}}^{\star}$ refers to p chains of integrators.
- The matrix $\bar{\boldsymbol{\Pi}}\bar{\boldsymbol{C}}$ can be considered as an output injection and, thus, can be easily taken into account by an observer.
- The matrix $\bar{\boldsymbol{P}}\bar{\boldsymbol{M}}$ contains the remaining couplings that can not be considered as an output injection. However, thanks to the suitable block structure - all elements on and above the block main diagonal are zero - these can be taken into account by an observer.

The existence of transformations to observer normal (2) is ensured by

Theorem 2.1 (transformation to obs. normal form [13]): Let system (1) be strongly observable. Then, there exist non-singular transformation matrices $\boldsymbol{T} \in \mathbb{R}^{n \times n}$ and $\boldsymbol{\Gamma} \in \mathbb{R}^{p \times p}$ such that the state transformation $\bar{\boldsymbol{x}} = \boldsymbol{T}^{-1}\boldsymbol{x}$ and the output transformation $\bar{\boldsymbol{y}} = \boldsymbol{\Gamma}\boldsymbol{y}$ yield the system in observer normal form (2). The orders of the subsystems given by the integers μ_j, $j = 1, \ldots, p$, are sorted in descending order, i.e.,

$$\mu_1 \geq \mu_2 \geq \cdots \geq \mu_p > 0. \tag{3}$$

In addition to the proof of Theorem 2.1, also a constructive algorithm for the transformation matrices $\boldsymbol{T}$ and $\boldsymbol{\Gamma}$ is presented in [13].

B. Observer Design in Observer Normal Form

Typically, sliding-mode based observers require

Assumption 2.1: The unknown inputs are bounded, i.e.,

$$|w_i(t)| \leq L_i \quad \forall t, \qquad 0 \leq L_i < \infty, \quad i = 1, \ldots, m. \tag{4}$$

The observer for system (2) is given by

$$\dot{\hat{\bar{\boldsymbol{x}}}} = \bar{\boldsymbol{A}}\hat{\bar{\boldsymbol{x}}} + \bar{\boldsymbol{\Pi}}\boldsymbol{\sigma}_{\bar{\boldsymbol{y}}} + \bar{\boldsymbol{l}}(\boldsymbol{\sigma}_{\bar{\boldsymbol{y}}}), \quad \hat{\bar{\boldsymbol{y}}} = \bar{\boldsymbol{C}}\hat{\bar{\boldsymbol{x}}}, \tag{5a}$$

where

$$\boldsymbol{\sigma}_{\bar{\boldsymbol{y}}} = \bar{\boldsymbol{y}} - \hat{\bar{\boldsymbol{y}}} = \begin{bmatrix} \sigma_1 & \sigma_{\mu_1+1} & \ldots & \sigma_{\mu_1+\cdots+\mu_{p-1}+1} \end{bmatrix}^{\mathrm{T}} \tag{5b}$$

is the output error and $\bar{\boldsymbol{l}}(\boldsymbol{\sigma}_{\bar{\boldsymbol{y}}})$ is some possibly nonlinear output injection. A reasonable choice of $\bar{\boldsymbol{l}}(\boldsymbol{\sigma}_{\bar{\boldsymbol{y}}})$ relying on Levant's RED is proposed in

Theorem 2.2 (finite-time observer [13]): Consider the observer (5) for the estimation of the state vector $\bar{\boldsymbol{x}}$ of system (2), the choice

$$\bar{\boldsymbol{l}}(\boldsymbol{\sigma}_{\bar{\boldsymbol{y}}}) = \begin{bmatrix} \kappa_{1,\mu_1-1}\lfloor\sigma_1\rceil^{\frac{\mu_1-1}{\mu_1}} \\ \vdots \\ \kappa_{1,1}\lfloor\sigma_1\rceil^{\frac{1}{\mu_1}} \\ \kappa_{1,0}\lfloor\sigma_1\rceil^{0} \\ \hline \vdots \\ \hline \kappa_{p,\mu_p-1}\lfloor\sigma_{\mu_1+\cdots+\mu_{p-1}+1}\rceil^{\frac{\mu_p-1}{\mu_p}} \\ \vdots \\ \kappa_{p,0}\lfloor\sigma_{\mu_1+\cdots+\mu_{p-1}+1}\rceil^{0} \end{bmatrix} \tag{6}$$

for the nonlinear output injection and the bounds L_i for the unknown inputs given in (4). Then, there exist parameters $\kappa_{j,k}$, $j = 1,\ldots,p$, $k = 0,\ldots,\mu_j-1$, such that the estimation error $\boldsymbol{\sigma} = \bar{\boldsymbol{x}} - \hat{\bar{\boldsymbol{x}}}$ converges to zero within finite time despite the unknown input for any initial states. Moreover, convergence of the observer for all admissible unknown input signals in terms of Assumption 2.1 is achieved only if $\kappa_{j,0} > \begin{bmatrix} L_1 & \ldots & L_m \end{bmatrix} |\bar{\boldsymbol{d}}_j|$.

The proof is given in [13]. □

Therein, it is shown that the dynamics of the estimation error $\boldsymbol{\sigma} = \begin{bmatrix} \sigma_1 & \ldots & \sigma_n \end{bmatrix}^{\mathrm{T}}$ are composed of p subsystems, each corresponding to the estimation error dynamics of an RED. For example, the j-th subsystem is given by

$$\begin{aligned} \dot{\sigma}_{\mu_1+\cdots+\mu_{j-1}+1} &= \sigma_{\mu_1+\cdots+\mu_{j-1}+2} - \\ &\qquad \kappa_{j,\mu_j-1}\lfloor\sigma_{\mu_1+\cdots+\mu_{j-1}+1}\rceil^{\frac{\mu_j-1}{\mu_j}} \\ &\vdots \\ \dot{\sigma}_{\mu_1+\cdots+\mu_j-1} &= \sigma_{\mu_1+\cdots+\mu_j} - \kappa_{j,1}\lfloor\sigma_{\mu_1+\cdots+\mu_{j-1}+1}\rceil^{\frac{1}{\mu_j}} \\ \dot{\sigma}_{\mu_1+\cdots+\mu_j} &= -\kappa_{j,0}\lfloor\sigma_{\mu_1+\cdots+\mu_{j-1}+1}\rceil^{0} + \boldsymbol{\beta}_j^{\mathrm{T}}\boldsymbol{\sigma} + \bar{\boldsymbol{d}}_j^{\mathrm{T}}\boldsymbol{w}, \end{aligned} \tag{7}$$

where $\boldsymbol{\beta}_j^{\mathrm{T}}\boldsymbol{\sigma} + \bar{\boldsymbol{d}}_j^{\mathrm{T}}\boldsymbol{w}$ acts as unknown input. If this unknown input is bounded, then there exist parameters $\kappa_{j,k}$ such that the respective error variables converge to zero within finite time [1]. Due to the advantageous structure of $\boldsymbol{\beta}_j^{\mathrm{T}}$, see (2c), $\boldsymbol{\beta}_j^{\mathrm{T}}\boldsymbol{\sigma}$ vanishes when all preceding subsystems have converged. Hence, the choice of $\kappa_{j,k}$ depends on the bounds of $\bar{\boldsymbol{d}}_j^{\mathrm{T}}\boldsymbol{w}$ only, which is bounded due to Assumption 2.1.

Note that in the case that $\bar{\boldsymbol{d}}_j = \boldsymbol{0}$, i.e., the corresponding subsystem is not affected by $\boldsymbol{w}$, the respective elements of $\bar{\boldsymbol{l}}(\boldsymbol{\sigma}_{\bar{\boldsymbol{y}}})$ may also be chosen in a different way. For instance, a linear choice leads to a linear observer for the respective subsystem which provides asymptotic convergence of the error variables.

III. Laboratory Setup and Problem Statement

In the following, the laboratory setup is presented and the estimation problem is formulated.

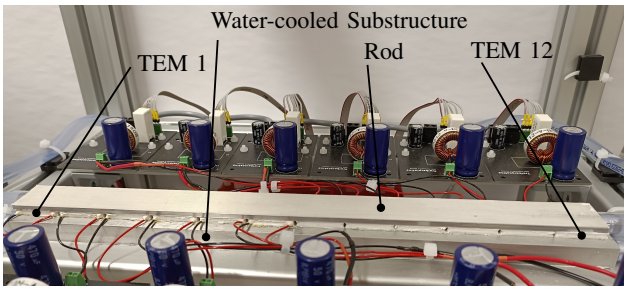

Fig. 1. The laboratory setup used for the experiments discussed in this paper. Twelve thermoelectric modules (TEMs) are mounted underneath an aluminium rod. The lower surface of the TEMs is kept at ambient temperature.

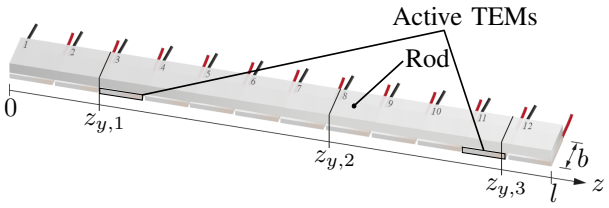

Fig. 2. The goal is to estimate the temperature profile of the rod along the z-axis from the temperature measurements at the positions $z_{y,1}$, $z_{y,2}$ and $z_{y,3}$ in the presence of unknown heat fluxes caused by TEM 3 and TEM 11. The figure is taken from [17, p. 11] and slightly modified with the author's permission.

A. Description of the Laboratory Setup

A detailed view of the considered laboratory setup is given in Fig. 1. The centrepiece is a uniformly shaped rod made of aluminium alloy `EN AW-6060` with length $l = 315$ mm, width $b = 25$ mm and thickness $d = 3$ mm. Along the rod, different thermal phenomena can be observed, such as heat conduction, convective heat loss and heat loss due to radiation.

In order to thermally excite the rod, $N_{\mathrm{TEM}} = 12$ so-called thermoelectric modules (TEMs) [15] are mounted at the bottom. Each TEM houses several thermocouples which, with the help of the Peltier effect [16], allow to introduce a heat flux into the rod at the mounting location. Depending on the direction of the applied electric current, the rod is either heated or cooled. A water-cooled substructure keeps the lower surface of the TEMs at ambient temperature T_{amb}, which enlarges the achievable temperature range of the TEMs. A thermal imaging camera with a resolutions of 120×160 pixels is installed on top, which allows to measure the rod temperature at any desired position at a rate of 10 frames per second.

B. Problem Statement

The estimation problem is sketched in Fig. 2. The objective is to estimate the rod's temperature profile along the z-axis from three punctual temperature measurements located at

$$z_{y,1} = 53.5 \text{ mm}, \quad z_{y,2} = 186.8 \text{ mm}, \quad z_{y,3} = 285.7 \text{ mm}. \tag{8}$$

These measurements correspond to three single pixels of the thermal imaging camera.

Furthermore, only TEM 3 and TEM 11 are actuated. The actuation, i.e., the supplied electric currents and the resulting generated heat fluxes, are considered unknown for the estimation algorithm to be designed. All other TEMs are not actuated.

To sum up, the goal is to design an observer that estimates the temperature profile from $p = 3$ available measurements in the presence of $m = 2$ unknown inputs corresponding to the heat fluxes of both actuated TEMs.

IV. Modelling

In order to describe the thermal behaviour along the aluminium rod, the physical effects of heat conduction, heat losses and the external heat input generated by the TEMs are considered. The resulting model takes the form of a PDE, which is then spatially discretized on a regular grid and, thus, is transferred into a finite-dimensional state-space model for the subsequent observer design.

A. Physical Modelling of the Rod

Due to symmetry of the system in transverse direction and because the rod is narrow compared to its length, i.e., $l \gg b$ and $l \gg d$, the heat transfer mainly takes place along the longitudinal direction (the z-axis introduced in Fig. 2) of the rod. Hence, the temperature is assumed to be constant over the cross-sectional. Further assuming constant material parameters, the temperature T of the rod is described by the one-dimensional heat equation, see [18, eqn. (2.244)]

$$\frac{\partial T(z,t)}{\partial t} = \frac{k}{c\rho}\frac{\partial^2 T(z,t)}{\partial z^2} + \frac{1}{c\rho}\dot{q}_V(z,t) \tag{9}$$

where k is the thermal conductivity, c is the specific heat capacity, ρ is the density of the rod material with the volumetric heat flux

$$\dot{q}_V(z,t) = \dot{q}_{V,\text{loss}}(z,t) + \sum_{j=1}^{N_\text{TEM}} \dot{q}_{V,\text{TEM},j}(z,t) \tag{10}$$

consisting of ambient heat losses $\dot{q}_{V,\text{loss}}$ and volumetric heat fluxes $\dot{q}_{V,\text{TEM},j}$ generated by the TEMs. Since radiation losses play a negligible role at the temperatures considered, a purely convective heat transfer is assumed for the ambient losses, i.e.,

$$\dot{q}_{V,\text{loss}}(z,t) = -h\frac{A}{V}\Big(T(z,t) - T_\text{amb}\Big), \tag{11}$$

where h describes the average heat transfer coefficient, A is the rod's surface area, V denotes the volume of the rod and T_amb is the ambient temperature. The heat generated by the TEMs is assumed to be uniformly distributed over the entire contact area. Thus, the volumetric heat flux of the j-th TEM is given by

$$\dot{q}_{V,\text{TEM},j}(z,t) = \dot{\tilde{q}}_{V,\text{TEM},j}(t) f_j(z), \tag{12}$$

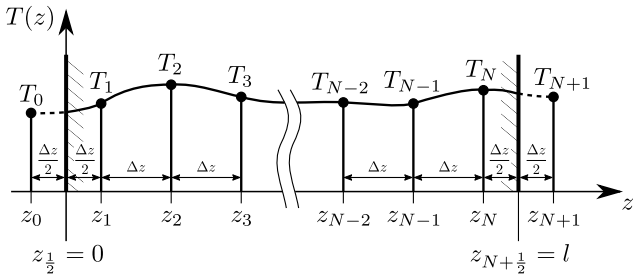

Fig. 3. Partitioning of the rod into a grid of N nodes inside of the rod for the spatial discretization of the PDE (9).

where $\dot{\tilde{q}}_{V,\text{TEM},j}(t)$ is the time-dependent volumetric heat flux and

$$f_j(z) = \begin{cases} 1 & \text{if } (j-1)\frac{l}{N_\text{TEM}} < z < j\frac{l}{N_\text{TEM}} \\ 0 & \text{else} \end{cases} \tag{13}$$

defines the position of the contact surface. It is noted that $\dot{\tilde{q}}_{V,\text{TEM},j}(t)$ could be considered as a function of the applied electric current, the rod temperature at the contact surface and the bottom temperature of the respective TEM. However, these dependencies are not modelled here. Both the volumetric heat flux and the electric current are unknown to the observer being designed. Therefore, modelling this relation would not add any further value for observer design purposes.

At the boundaries, a convective heat transfer to the ambient air according to [18, eqn. (2.23)] is considered, which yields

$$\begin{aligned} \left.\frac{\partial T(z,t)}{\partial z}\right|_{z=0} &= \frac{\tilde{h}}{k}\Big(T(0,t) - T_\text{amb}\Big), \\ \left.\frac{\partial T(z,t)}{\partial z}\right|_{z=l} &= -\frac{\tilde{h}}{k}\Big(T(l,t) - T_\text{amb}\Big), \end{aligned} \tag{14}$$

where $\tilde{h}$ is the corresponding heat transfer coefficient[2].

B. Spatial Discretization of the Partial Differential Equation

The distributed parameter system (9)–(14) is spatially discretized following [18, Chapter 2.4.1][3]. As depicted in Fig. 3, temperatures $T_i(t) = T(z_i,t)$ at $N+2$ discrete positions

$$z_i = -\frac{\Delta z}{2} + i \cdot \Delta z, \qquad i = 0, \ldots, N+1, \tag{15}$$

are considered, where $\Delta z = \frac{l}{N}$.

In each position, the spatial derivatives are substituted by difference quotients. This, together with the discretization of the boundary conditions, results in a system of N first-order ordinary differential equations (ODEs).[4]

[2]Note that the heat transfer coefficients h and $\tilde{h}$ do not coincide. On the one hand, h additionally takes into account the rod's bottom side with the heat transfer to the TEMs. On the other hand, the orientation of the surface also plays a significant role in the heat transfer. In contrast to the top surface of the rod, the heated air can rise along the side surfaces. This behaviour leads to an increased heat transfer at the side surfaces.

[3]In contrast to [18, Chapter 2.4.1], no discretization in time but only spatial discretization is considered here.

[4]The nodes located at z_0 and z_{N+1} outside the rod are used for the discretization the boundary conditions. This reduces the number of ODEs to N.

C. Model Parameters

The number of nodes for the spatial discretization is chosen as $N = 156$, which has proven to be sufficiently large w.r.t. the resulting discretization error, see Section VI-B. Furthermore, due to the position and the resolution of the thermal imaging camera, the distance between two adjacent pixels corresponds exactly to the discretization width Δz, which allows for a straightforward validation of the node temperatures estimated by the observer to be designed.

The density $\rho = 2700\ \mathrm{kg/m^3}$, the thermal conductivity $k = 209\ \mathrm{W/(m \cdot K)}$ and the specific heat capacity $c = 898\ \mathrm{J/(kg \cdot K)}$ of the rod material[5] were taken from tables in the literature [19, pp. 634 and 637] and a data sheet [20][6]. The heat transfer coefficients $h = 48.2\ \mathrm{W/(m^2 \cdot K)}$ and $\tilde{h} = 1982\ \mathrm{W/(m^2 \cdot K)}$ were determined from a cool-down experiment by minimizing a quadratic cost function. The ambient temperature $T_{\mathrm{amb}} = 25°\mathrm{C}$ was measured at the beginning of the experiment and is assumed constant hereafter.

D. Representation as Continuous-Time State-Space Model

The spatially discretized PDE model is summarized in the form of an LTI continuous-time state space model. To get rid of the dependency of the model on the constant ambient temperature T_{amb} the state state vector

$$\boldsymbol{\theta} = \begin{bmatrix} \theta_1 & \dots & \theta_{156} \end{bmatrix}^{\mathrm{T}} = \begin{bmatrix} T_1 - T_{\mathrm{amb}} & \dots & T_{156} - T_{\mathrm{amb}} \end{bmatrix}^{\mathrm{T}} \tag{16}$$

is defined. Furthermore, the vector of unknown inputs $\boldsymbol{w} = \begin{bmatrix} \dot{\tilde{q}}_{V,\mathrm{TEM},3} & \dot{\tilde{q}}_{V,\mathrm{TEM},11} \end{bmatrix}^{\mathrm{T}}$, the output vector $\boldsymbol{y} \overset{(8)}{=} \begin{bmatrix} \theta_{27} & \theta_{93} & \theta_{142} \end{bmatrix}^{\mathrm{T}}$ and insertion of the model parameters in coherent SI-units yields the LTI system

$$\frac{\mathrm{d}\boldsymbol{\theta}}{\mathrm{d}t} = \boldsymbol{A}_\theta \boldsymbol{\theta} + \boldsymbol{D}_\theta \boldsymbol{w}, \quad \boldsymbol{y} = \boldsymbol{C}_\theta \boldsymbol{\theta}, \tag{17a}$$

with the dynamic matrix[7]

$$\boldsymbol{A}_\theta = \begin{bmatrix} -21.61 & 21.20 & 0 & \dots & \dots & 0 \\ 21.14 & -42.30 & 21.14 & \ddots & & \vdots \\ 0 & 21.14 & -42.30 & 21.14 & \ddots & \vdots \\ \vdots & \ddots & \ddots & \ddots & \ddots & 0 \\ \vdots & & \ddots & 21.14 & -42.30 & 21.14 \\ 0 & \dots & \dots & 0 & 21.20 & -21.61 \end{bmatrix}, \tag{17b}$$

the unknown-input matrix

$$\boldsymbol{D}_\theta = 41.24 \cdot 10^{-6} \cdot \begin{bmatrix} \boldsymbol{d}_{\theta,1} & \boldsymbol{d}_{\theta,2} \end{bmatrix}, \tag{17c}$$

with columns $\boldsymbol{d}_{\theta,1} = \begin{bmatrix} \boldsymbol{0}_{1\times 26} & \boldsymbol{1}_{1\times 13} & \boldsymbol{0}_{1\times 117} \end{bmatrix}^{\mathrm{T}}$ and $\boldsymbol{d}_{\theta,2} = \begin{bmatrix} \boldsymbol{0}_{1\times 130} & \boldsymbol{1}_{1\times 13} & \boldsymbol{0}_{1\times 13} \end{bmatrix}^{\mathrm{T}}$, and the output matrix

$$\boldsymbol{C}_\theta = \begin{bmatrix} \boldsymbol{e}_{27}^{\mathrm{T}} \\ \boldsymbol{e}_{93}^{\mathrm{T}} \\ \boldsymbol{e}_{142}^{\mathrm{T}} \end{bmatrix}. \tag{17d}$$

[5]Aluminium alloy with material number `EN AW-6060`.

[6]Due to an obviously wrong value, the specific heat capacity could not be taken from [19, p. 639].

[7]The values are rounded to two decimal places.

V. Observer Design for Estimation of the Temperature Profile

Prior to the observer design, a model order reduction is applied to (17). The resulting lower-order system is transformed into the observer normal form and the observer is designed.

A. Modal Model Order Reduction

The high order renders system (17) numerically unsuitable for the observer design. Hence, a modal model order reduction is applied that keeps the slow parts of the dynamics only. A transformation $\boldsymbol{\xi} = \begin{bmatrix} \boldsymbol{\xi}_1 & \boldsymbol{\xi}_2 \end{bmatrix}^{\mathrm{T}} = \boldsymbol{T}_\xi \boldsymbol{\theta}$ to diagonal form represents the system by means of $N = 156$ decoupled first order dynamics, where $\boldsymbol{\xi}_1$ corresponds to the slow modes[8] to be kept and $\boldsymbol{\xi}_2$ refers to the fast decaying modes to be approximated. The four slowest modes are assigned to $\boldsymbol{\xi}_1$ whereas the remaining ones are approximated with a quasi-static approximation as discussed in [21, p. 285] and [22]. To reconstruct $\boldsymbol{\xi}$ it is not sufficient to estimate $\boldsymbol{\xi}_1$ only, but also $\boldsymbol{\xi}_2$ which requires an estimate of $\boldsymbol{w}$. Hence, the state vector of the reduced order system is augmented with $\boldsymbol{w}$ and its derivative $\dot{\boldsymbol{w}}$.

B. Transformation to Observer Normal Form

The resulting system of order $n = 8$ is transformed to observer normal form (2), which yields

$$\dot{\bar{\boldsymbol{x}}} = \bar{\boldsymbol{A}}\bar{\boldsymbol{x}} + \bar{\boldsymbol{D}}\ddot{\boldsymbol{w}}, \quad \bar{\boldsymbol{y}} = \bar{\boldsymbol{C}}\bar{\boldsymbol{x}}, \tag{18a}$$

where

$$\bar{\boldsymbol{A}} = \left[\begin{array}{cccc|cc|cc} 0.0367 & 1 & 0 & 0 & -0.5349 & 0 & 6.4194 & 0 \\ 0.0105 & 0 & 1 & 0 & 0.0076 & 0 & 1.7116 & 0 \\ -0.0135 & 0 & 0 & 1 & 0.0111 & 0 & 0.0602 & 0 \\ -0.0010 & 0 & 0 & 0 & 0.0004 & 0 & -0.0027 & 0 \\ \hline 0.1009 & 0 & 0 & 0 & 0.1616 & 1 & 0.2309 & 0 \\ -0.0247 & 0 & -0.4470 & 2.2258 & 0.0173 & 0 & -0.6042 & 0 \\ \hline 0.0063 & 0 & 0 & 0 & 0.0280 & 0 & -0.4080 & 1 \\ -0.0005 & 0 & -0.0681 & 0.0592 & -0.0003 & 0 & -0.1104 & 0 \end{array}\right],$$

$$\bar{\boldsymbol{D}} = 10^{-4} \cdot \left[\begin{array}{cc} 0 & 0 \\ 0 & 0 \\ 0 & 0 \\ 0 & 0 \\ \hline 0 & 0 \\ 52.4 & -3.0 \\ \hline 0 & 0 \\ 7.7 & 3.7 \end{array}\right], \quad \bar{\boldsymbol{C}} = \left[\begin{array}{cccc|cc|cc} 1 & 0 & 0 & 0 & 0 & 0 & 0 & 0 \\ 0 & 0 & 0 & 0 & 1 & 0 & 0 & 0 \\ 0 & 0 & 0 & 0 & 0 & 0 & 1 & 0 \end{array}\right]. \tag{18b}$$

The system in observer normal form (18a) has $m = 2$ unknown inputs $\ddot{\boldsymbol{w}}$ and $p = 3$ outputs. It consists of $p = 3$ coupled subsystems, each with a single output. The second and the third subsystem of order $\mu_2 = \mu_3 = 2$ are directly affected by $\ddot{\boldsymbol{w}}$, whereas the first subsystem of order $\mu_1 = 4$ is not.

[8]Characterized by the eigenvalues of the asymptotically stable system with the smallest absolute value of the real part.

C. Unknown Input Observer Design

As proposed in Section II, an observer of the form (5) is designed. The remaining task deals with the choice of the nonlinear output injection $\bar{\boldsymbol{l}}(\boldsymbol{\sigma}_{\bar{\boldsymbol{y}}})$. As discussed previously, the first subsystem is not directly affected by the unknown inputs. For this reason, the application of a linear observer for this subsystem is sufficient for asymptotic convergence, whereas an RED-based output injection is applied to the second and the third subsystem, which yields

$$\bar{\boldsymbol{l}}(\boldsymbol{\sigma}_{\bar{\boldsymbol{y}}}) = \begin{bmatrix} \kappa_{1,3}\sigma_1 \\ \kappa_{1,2}\sigma_1 \\ \kappa_{1,1}\sigma_1 \\ \kappa_{1,0}\sigma_1 \\ \hline \kappa_{2,1}\lfloor\sigma_5\rceil^{\frac{1}{2}} \\ \kappa_{2,0}\lfloor\sigma_5\rceil^{0} \\ \hline \kappa_{3,1}\lfloor\sigma_7\rceil^{\frac{1}{2}} \\ \kappa_{3,0}\lfloor\sigma_7\rceil^{0} \end{bmatrix}. \tag{19}$$

VI. Experimental Results

The discrete-time implementation of the observer applied in the laboratory follows the ideas of the so-called matching approach for the discretization of homogenous differentiators [23], [24], which allows for eliminating the discretization chattering phenomenon.

A. Experimental Procedure

The electric currents (in Ampere) of TEM 3 and TEM 11 were chosen

$$\begin{aligned} i_3(t) &= -0.6 + 0.4\sin\left(\frac{2\pi}{221}(t+t_0)\right), \\ i_{11}(t) &= 0.6 + 0.15\cos\left(\frac{2\pi}{100}(t+t_0)\right), \end{aligned} \tag{20}$$

respectively, where t_0 is some random time shift. Since the respective electrical current i_3 is negative, TEM 3 is in cooling mode, whereas TEM 11 is in heating mode. As the electrical currents and their derivatives are bounded, also the unknown inputs are bounded, which follows from [15].

For the linear observer of subsystem 1, purely real eigenvalues were assigned, which are uniformly distributed between -0.3 and -0.2, which yields $\kappa_{1,0} = 0.0037$, $\kappa_{1,1} = 0.0611$, $\kappa_{1,2} = 0.3722$ and $\kappa_{1,3} = 1$. The RED-based observers for subsystems 2 and 3 were chosen according to [25, Section 6.7]. As the bounds for the unknown inputs $\ddot{\boldsymbol{w}}$ are unknown, the scaling parameter has been increased until convergence of the respective output errors σ_5 and σ_7, which yields $\kappa_{2,0} = 0.44$, $\kappa_{2,1} = 0.9487$, $\kappa_{3,0} = 0.22$ and $\kappa_{3,1} = 0.6708$. The initial estimate of the temperature profile $\hat{T}_i$ is set to $\hat{T}_i(t=0) = 18°\text{C}$, $i = 1, \ldots, 156$. The initial values for the estimate $\hat{\boldsymbol{w}}$ and its derivative $\dot{\hat{\boldsymbol{w}}}$ are set to $\hat{\boldsymbol{w}}(t=0) = \dot{\hat{\boldsymbol{w}}}(t=0) = \boldsymbol{0}$. Individual pixels of the thermal camera, which are located in the centre of the rod, serve as measurements for the observer as well as for its validation.

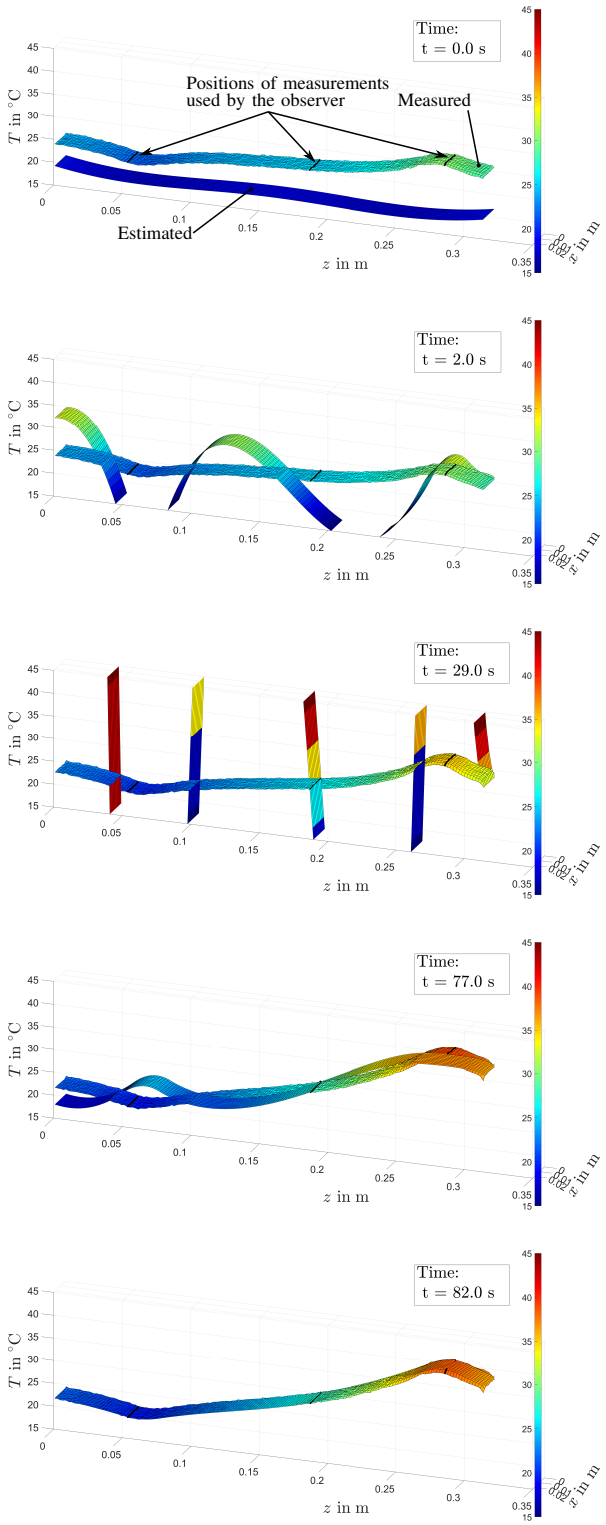

Fig. 4. Comparison of the measured and the estimated temperature profile along the aluminium rod at $t = 0$ s, $t = 2$ s, $t = 29$ s, $t = 77$ s and $t = 82$ s. After approximately 82 s the temperature profile estimate has converged to the actual temperature profile.

B. Estimation Results

Fig. 4 depicts the convergence of the observer estimates $\hat{T}_i$ to the actually measured temperatures T_i. Since the thermal imaging camera provides two-dimensional pictures, the measured rod temperature is represented as surface, where the height indicates the local temperature. In order to comparably represent the observer estimates, which actually correspond to a line in longitudinal direction, they are stretched in transverse direction. The position of the measurements used by the observer are indicated by black lines. Due to the applied model order reduction, the initial estimate can not be represented as a constant temperature of $18°\mathrm{C}$, but shows some small deviations. Furthermore, the initial estimation is far off the actual temperature profile, also on average, which leads to strong transients. After approximately 82 s the observer provides an accurate estimation. Fig. 5 shows a comparison of the temperature measurements T_i and its respective estimates $\hat{T}_i$ at two exemplary positions distributed along the rod. Again, it becomes apparent that the estimates approximate the actual temperatures well after the transients phase. It is noticeable that the estimate of T_9 located close to the rod boundary has a lower accuracy than the one located further inside.

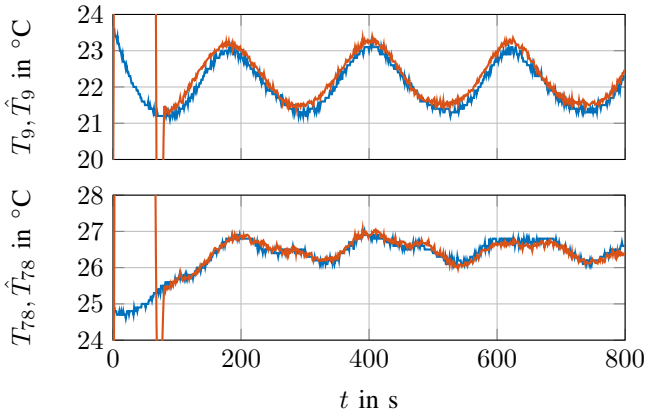

Fig. 5. Comparison of measurements T_i and estimates $\hat{T}_i$ at two exemplary positions (out of $N = 156$ node positions in total) along the rod.

VII. Conclusion

The recently proposed observer design method [13] for LTI multivariable systems with unknown inputs has been successfully applied for the temperature profile estimation of an aluminium rod which is exposed to unknown heat fluxes. It was demonstrated that, due the advantageous structure of the observer normal form, the observer design is simple and intuitive. The experimental results validate both the accuracy of the provided observer in estimating the rod's temperature profile and the practicality of the proposed observer design method.

Acknowledgment

The authors would like to thank Andreas Johannes Anabith for permission to use Fig. 2 in a slightly modified form from his master's thesis.

References

[1] A. Levant, "Higher-order sliding modes, differentiation and output-feedback control," *International Journal of Control*, vol. 76, no. 9-10, pp. 924–941, 2003.

[2] T. Floquet, C. Edwards, and S. K. Spurgeon, "On sliding mode observers for systems with unknown inputs," *International Journal of Adaptive Control and Signal Processing*, vol. 21, no. 8-9, pp. 638–656, 2007.

[3] J. Davila, L. Fridman, A. Pisano, and E. Usai, "Finite-time state observation for non-linear uncertain systems via higher-order sliding modes," *International Journal of Control*, vol. 82, no. 8, pp. 1564–1574, 2009.

[4] L. Fridman, A. Levant, and J. Davila, "Observation of linear systems with unknown inputs via high-order sliding-modes," *International Journal of systems science*, vol. 38, no. 10, pp. 773–791, 2007.

[5] Y. Shtessel, C. Edwards, L. Fridman, and A. Levant, *Sliding mode control and observation*, vol. 10. Springer, 2014.

[6] M. Tranninger, R. Seeber, M. Steinberger, and M. Horn, "Exact State Reconstruction for LTI-Systems with Non-Differentiable Unknown Inputs," in *2019 18th European Control Conference (ECC)*, pp. 3096–3102, IEEE, 2019.

[7] M. L. Hautus, "Strong detectability and observers," *Linear Algebra and its Applications*, vol. 50, pp. 353–368, 1983.

[8] C. Edwards and S. Spurgeon, *Sliding mode control: theory and applications*. Crc Press, 1998.

[9] B. Walcott and S. Zak, "State observation of nonlinear uncertain dynamical systems," *IEEE Transactions on Automatic Control*, vol. 32, no. 2, pp. 166–170, 1987.

[10] M. Darouach, M. Zasadzinski, and S. J. Xu, "Full-order observers for linear systems with unknown inputs," *IEEE Transactions on Automatic Control*, vol. 39, no. 3, pp. 606–609, 1994.

[11] H. Ríos, M. Mera, D. Efimov, and A. Polyakov, "Robust output-control for uncertain linear systems: Homogeneous differentiator-based observer approach," *International Journal of Robust and Nonlinear Control*, vol. 27, no. 11, pp. 1895–1914, 2017.

[12] J. Davila, M. Tranninger, and L. Fridman, "Finite-time state-observer for a class of linear time-varying systems with unknown inputs," *IEEE Transactions on Automatic Control*, 2021.

[13] H. Niederwieser, M. Tranninger, R. Seeber, and M. Reichhartinger, "Unknown input observer design for linear time-invariant multivariable systems based on a new observer normal form," *International Journal of Systems Science*, vol. 53, no. 10, pp. 2180–2206, 2022.

[14] A. Filippov, *Differential Equations with Discontinuous Righthand Sides - Control Systems*. Berlin Heidelberg: Springer Science & Business Media, 2013.

[15] C. Alaoui, "Peltier thermoelectric modules modeling and evaluation," *International Journal of Engineering (IJE)*, vol. 5, pp. 114–121, 2011.

[16] W. Brostow, G. Granowski, N. Hnatchuk, J. Sharp, and J. B. White, "Thermoelectric phenomena," *Journal of Materials Education*, vol. 36, pp. 175–185, 2014.

[17] A. Anabith, *Late-Lumping Controller Synthesis for a Heated Rod with Boundary Actuation*. Master's Thesis, Institute of Automation and Control, University of Technology Graz, May 2022.

[18] H. D. Baehr and K. Stephan, *Wärme-und Stoffübertragung*, vol. 5. Springer, 2006.

[19] Verein deutscher Ingenieure, *VDI-Wärmeatlas*. Berlin Heidelberg: Springer, 11 ed., 2013.

[20] Thyssenkrupp Materials (UK) Ltd, "Aluminium 6060." https://www.thyssenkrupp-materials.co.uk/aluminium-6060.html (accessed 2023-05-14), 2023.

[21] A. C. Antoulas, *Approximation of large-scale dynamical systems*. SIAM, 2005.

[22] K. Fernando and H. Nicholson, "Singular perturbational model reduction in the frequency domain," *IEEE Transactions on Automatic Control*, vol. 27, no. 4, pp. 969–970, 1982.

[23] S. Koch and M. Reichhartinger, "Discrete-time equivalent homogeneous differentiators," in *2018 15th International Workshop on Variable Structure Systems (VSS)*, pp. 354–359, IEEE, 2018.

[24] M. Reichhartinger, S. Koch, H. Niederwieser, and S. K. Spurgeon, "The robust exact differentiator toolbox: Improved discrete-time realization," in *2018 15th International Workshop on Variable Structure Systems (VSS)*, pp. 1–6, IEEE, 2018.

[25] Y. Shtessel, C. Edwards, L. Fridman, and A. Levant, *Sliding mode control and observation*. Springer, 2014.